AGU PUBLICATIONS

JGR

Journal of Geophysical Research: Oceans

RESEARCH ARTICLE

10.1002/2017JC012941

Influence of Sea Ice Crack Formation on the Spatial Distribution of Nutrients and Microalgae in Flooded Antarctic Multiyear Ice

Daiki Nomura[1,2,3,4], Shigeru Aoki[1], Daisuke Simizu[2], and Takahiro Iida[2,3]

[1]Institute of Low Temperature Science, Hokkaido University, Sapporo, Japan, [2]National Institute of Polar Research, Tachikawa, Japan, [3]Faculty of Fisheries Sciences, Hokkaido University, Hakodate, Japan, [4]Arctic Research Center, Hokkaido University, Sapporo, Japan

Key Points:
- Cracks in sea ice resulted in high chlorophyll concentrations in slush up to a few meters from the crack
- The 64–84% of the crack water consisted of snow meltwater supplied during the melt season
- Nutrient and chl *a* within slush revealed the intrusion of water from the crack

Supporting Information:
- Table S1
- Table S2
- Table S3

Correspondence to:
D. Nomura,
daiki.nomura@fish.hokudai.ac.jp

Citation:
Nomura, D., Aoki, S., Simizu, D., & Iida, T. (2018). Influence of sea ice crack formation on the spatial distribution of nutrients and microalgae in flooded Antarctic multiyear ice. *Journal of Geophysical Research: Oceans*, *123*, 939–951. https://doi.org/10.1002/2017JC012941

Received 29 MAR 2017
Accepted 9 JAN 2018
Accepted article online 19 JAN 2018
Published online 6 FEB 2018

Abstract Cracks are common and natural features of sea ice formed in the polar oceans. In this study, a sea ice crack in flooded, multiyear, land-fast Antarctic sea ice was examined to assess its influence on biological productivity and the transport of nutrients and microalgae into the upper layers of neighboring sea ice. The water inside the crack and the surrounding host ice were characterized by a strong discoloration (brown color), an indicator of a massive algal bloom. Salinity and oxygen isotopic ratio measurements indicated that 64–84% of the crack water consisted of snow meltwater supplied during the melt season. Measurements of nutrient and chlorophyll *a* concentrations within the slush layer pool (the flooded layer at the snow-ice interface) revealed the intrusion of water from the crack, likely forced by mixing with underlying seawater during the tidal cycle. Our results suggest that sea ice crack formation provides conditions favorable for algal blooms by directly exposing the crack water to sunlight and supplying nutrients from the under-ice water. Subsequently, constituents of the crack water modified by biological activity were transported into the upper layer of the flooded sea ice. They were then preserved in the multiyear ice column formed by upward growth of sea ice caused by snow ice formation in areas of significant snow accumulation.

Plain Language Summary Formation of cracks in sea ice affects the environment associated with biological production and biogeochemical cycling in the surface ocean of sea ice systems. Because cracks are likely to form frequently within the sea ice during the season of ice melting and ice breaking, the contributions of cracks to biological production and biogeochemical cycling may be significant in ice-covered oceans. In the future, the melting of sea ice in polar oceans will strongly affect the output of biogeochemical parameters trapped within sea ice and their use in primary and secondary production within surface oceans. In the case of multiyear, land-fast ice, biogeochemical parameters that accumulate within the ice would be discharged abruptly to ocean surface waters when the multiyear ice breaks up.

1. Introduction

Sea ice crack formation affects physical, chemical, and biological processes that take place at the interface between the ocean and atmosphere. From a physical perspective, a crack affects the heat budget at the ocean-atmosphere interface when it refreezes (Petrich et al., 2007) because sea ice impedes the exchange of heat with the atmosphere (Maykut, 1978). Moreover, an open crack acts as an active site for gas exchange between the ocean and atmosphere (Loose et al., 2014; Steiner et al., 2013;). Crack formation is also relevant to atmospheric chemistry. For instance, crack formation has been shown to influence the dynamics of ozone and mercury in the Arctic boundary layer (Moore et al., 2014). From a biological perspective, the sudden formation of a crack exposes algae in the sea ice and water immediately below the ice to sunlight. Generally, photosynthesis is light limited in the middle and bottom layers of sea ice and in water beneath sea ice (Ehn et al., 2008). Therefore, the supply of sunlight through cracks in the ice can modify the amount and spectral characteristics of light that reach the algal communities and affect biological productivity in polar oceans. The fact that cracks are common and natural features of sea ice formed in polar oceans (Willmes & Heinemann, 2016) suggests that crack formation is an important process in the sea ice environment.

If a heavy load of snow depresses the snow-ice interface below sea level, the sea ice will be flooded. Snow loading and the formation of snow-ice and superimposed ice lead to the formation of a horizontal surface

slush layer between the snow and sea ice (Ackley et al., 2008; Eicken et al., 1994; Haas et al., 2001; Jeffries et al., 2001; Jutras et al., 2016). During the formation of a slush layer, water is supplied to the layer by horizontal movement from the edge of the ice floe and through upward percolation of seawater through openings in the sea ice where the sea ice is fractured (Golden et al., 1998; Haas et al., 2001; Perovich et al., 2004). Extensive algal production has been observed within the sea ice surface (Ackley & Sullivan, 1994; Fritsen et al., 1994; Kattner et al., 2004; Schnack-Schiel et al., 2001). In the slush layer, high biological activity and the supply of meltwater from snow and ice-surface melting (Nomura el al., 2012a, 2013) alter the biogeochemical properties of the slush layer, although water exchange also occurs with ambient seawater by wave action (Ackley et al., 2008; Haas et al., 2001). Such slush layers form much more frequently over Antarctic sea ice than over Arctic sea ice because snow accumulation is greater in the Antarctic sea ice zone (Ackley et al., 2008; Haas et al., 2001; Kattner et al., 2004; Nomura et al., 2013; Papadimitriou et al., 2009; Zemmelink et al., 2008). Subsequent freezing of the slush layer when the heat is lost and the temperature falls below the freezing point promotes the formation of snow ice (Kawamura et al., 1997; Maksym & Jeffries, 2000). During the formation of snow ice, the slush water, along with any chemical and biological materials it contains, is incorporated into the sea ice. The repetition of this process each year can result in an increase of the thickness of multiyear ice, within which any included chemical and biological materials can be preserved for a long time.

This study was a first step toward understanding the effect of sea ice crack formation on the physical, chemical, and biological processes in crack water and subsequent process of incorporation of biogeochemical constituents into the slush water and multiyear sea ice through snow-ice formation. The experimental design included field measurements focused primarily on biological production and processes in crack water and the horizontal transport of biological materials (nutrients and algae) from cracks to slush layers that form in multiyear ice. We also examined sea ice cores to quantify the rates of photosynthesis and remineralization during storage within the sea ice.

2. Materials and Methods

Sea ice crack observations were carried out during the 51st Japanese Antarctic Research Expedition over multiyear land-fast ice in Lützow-Holm Bay, Eastern Antarctica, in January 2010 (Figure 1 and supporting information Table S1). In this area, the last complete breakup of the fast ice cover occurred during March 1980 (Higashi et al., 1982; Ushio, 2006). During the study period, a crack about 250 m long developed in a direction perpendicular to the edge of the Ongul Islands. Water from that crack was sampled at 10 stations (Stations C1–10) along the whole length of the crack (Figure 1). An ice station (M1) was established about 400 m away from the crack site in the multiyear land-fast ice area (Figure 1) so that sea ice properties at the crack site could be compared with those at a site with no crack. The area where sea ice research was conducted in this study was flooded as a result of the negative freeboard and it included no surface melt ponds.

To sample the water in the sea ice crack at C1–10, 0.05 × 0.05 m holes were cut through thin (about 0.01 m) refrozen surface ice with a hand saw. Surface water in the crack was then pumped out through the hole with a diaphragm pump (EWP-01, As One Corporation, Osaka, Japan) from a depth of 0.3 m and dispensed into (1) a 12 mL glass screw-cap vial (Nichiden-Rika Glass Co. Ltd, Kobe, Japan) for measurement of salinity and oxygen isotopic ratio ($\delta^{18}O$), (2) a 500 mL Nalgene polycarbonate bottle (Thermo Fisher Scientific Inc., Waltham, MA) for measurement of chlorophyll *a* (chl *a*), and (3) a 10 mL polyethylene screw-cap vial (Eiken Chemical Co. Ltd, Tokyo, Japan) for measurement of inorganic nutrient concentrations ($NO_3^- + NO_2^-$, NH_4^+, and PO_4^{3-}). For microscopic examination of algal species, water was collected from the sea ice crack at C5 and dispensed into a 500 mL Nalgene polycarbonate bottle (Thermo Fisher Scientific Inc.). An aliquot of 5 mL of Lugol's solution was added to preserve the algal samples.

Snow on sea ice was sampled with a polyethylene shovel (GL Science Inc., Tokyo, Japan) at three depths at C7 (0.5 m away from the edge of the crack) and at M1 and dispensed into polyethylene cups (GL Science Inc.; Figure 1 and supporting information Table S1). Slush water was collected at distances of 1, 2, 3, 4, 5, and 10 m away from the edge of the crack at C5 (points S1, 2, 3, 4, 5, and 10, respectively, in Figure 2) to examine the horizontal gradient of slush water properties near the crack (Figures 1 and 2 and supporting information Table S1). Slush water was also collected at C7 (0.5 m away from the edge of the crack) and M1.

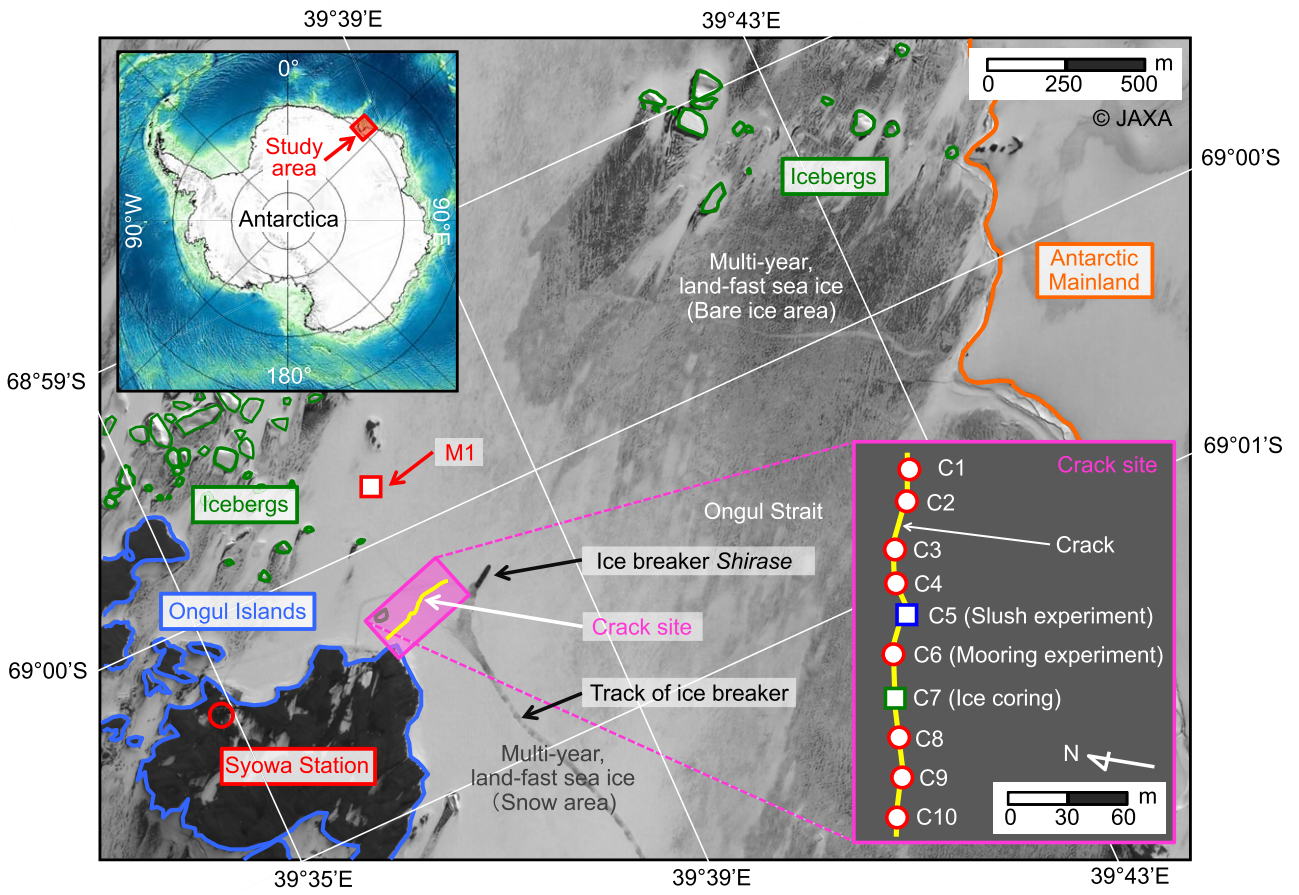

Figure 1. Location of the sampling area in Lützow-Holm Bay, Eastern Antarctica. This Advanced Land Observing Satellite (ALOS)/the Panchromatic Remote-sensing Instrument for Stereo Mapping (PRISM) image was obtained on 26 January 2010 from Japan Aerospace Exploration Agency (JAXA). Green, blue, and orange lines indicate icebergs, Ongul Island, and the Antarctic continent, respectively. Pink area indicates the crack site. Details of the station locations along the crack are shown in the inset (lower right). The darker area sea ice area in the Ongul Strait corresponds to the area of bare ice that is thinning during the ice melt season.

The superimposed ice (about 10 cm, as reported by Nomura et al. (2012a)) was scraped with a polyethylene shovel. Then, to sample the slush water, snow and superimposed ice were carefully removed from an area of 0.5 m × 0.5 m without disturbing the slush layer. The slush water was then collected with a diaphragm pump for measurements of salinity, $\delta^{18}O$, chl *a*, and inorganic nutrients. Slush water depth (from sea level to sea ice surface) was measured using a ruler.

Sea ice cores were collected at C7 (0.5 m away from the edge of the crack) and M1 (Figure 1 and supporting information Table S1). At each station, two ice cores were sampled using an ice corer (Geo Tecs Co., Ltd., Chiba, Japan) with an internal diameter of 0.09 m. The first ice core for bulk ice salinity, $\delta^{18}O$, nutrient concentrations, and sea ice texture was immediately placed in a polyethylene tube and kept in a horizontal position in a cooler box along with refrigerants to keep its temperature low and to minimize brine drainage from the core. The second core for bulk ice chl *a* concentration was sliced into 0.2 m-thick sections with a hand saw on site, and the samples were placed in polyethylene cups (GL Science Inc.).

Under-ice water was collected through ice core holes with a Teflon water sampler (GL Science Inc.) from 1 and 7 m below the bottom of the sea ice at C7 and M1 (Figure 1 and supporting information Table S1). Under-ice water samples were collected approximately 30 min after the ice core was drilled to avoid potential artifacts associated with the disturbance caused by drilling. Samples were collected in the same manner as the slush water samples.

Memory-type conductivity-temperature (CT) sensors (Compact CT, JFE Advantech Co., Ltd., Hyogo, Japan) were suspended with a line supported by a tripod on the sea ice and moored in the middle of the crack

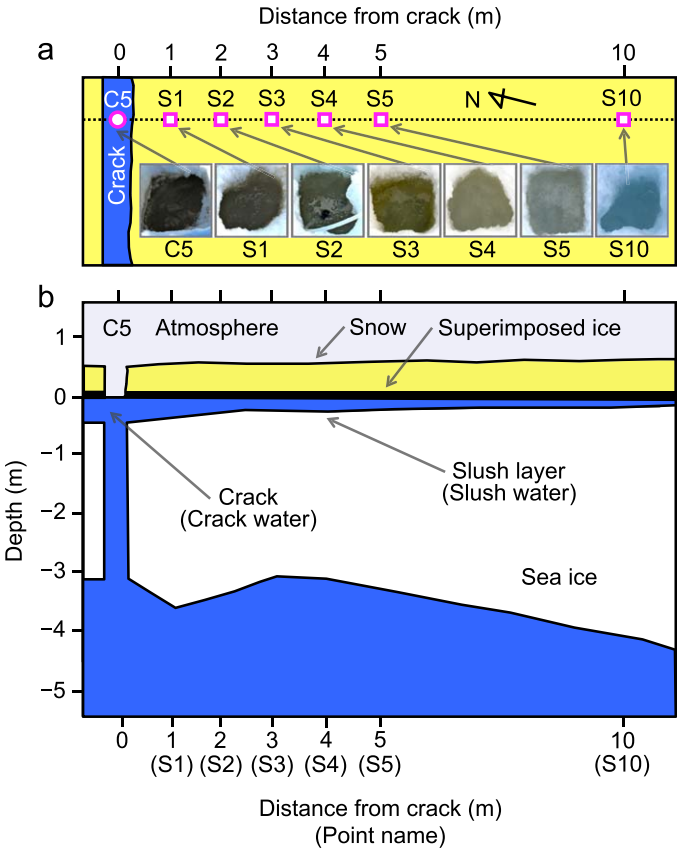

Figure 2. (a) Schematic illustrations of overhead pictures of the crack and slush layer at C5. For the slush layer, overhead pictures were taken after removing the snow and cutting the hole over the superimposed ice. (b) Schematic illustration of vertical cross section of the crack and slush layer through S1–10 at C5.

water at depths of 0.3 and 0.6 m from the water surface at C6 (Figure 1) to monitor the temporal variation of water temperature and salinity in the crack from 27 January to 31 January. Time series of sea level, air temperature, wind speed, and solar radiation were obtained at Syowa Station and were used to interpret the heat and freshwater changes of the crack water at C6. Water depths at each station were measured using fishing line with a sinker (diameter, 1 cm; length, 5 cm) through the crack at C1–9 and the ice core hole at M1.

All samples collected were brought back to the laboratory of the Japan Maritime Self-Defense Force icebreaker Shirase (Figure 1) and stored until analysis. Samples for salinity and $\delta^{18}O$ were stored in a refrigerator (4°C). Samples for nutrient concentrations were stored in a freezer (−30°C) without filtration. Slush and under-ice water samples for chl *a* measurements were immediately filtered through 25 mm-diameter Whatman GF/F filters in the laboratory. Chlorophyll pigments on the filters were then extracted with dimethylformamide (Suzuki & Ishimaru, 1990) for 24 h in a −80°C freezer.

In the Shirase cold room (−20°C), the first ice core was split lengthwise into two halves with an electric band saw. The first half was used for measurement of ice salinity, $\delta^{18}O$, and nutrient concentrations; the second half was used for ice texture analysis. For measurement of ice salinity, $\delta^{18}O$, and nutrient concentrations, the first half was cut into a 0.045 m × 0.025 m rectangular cross section and then sliced into 0.2 m-thick sections. To avoid contamination during sampling and handling, the outer 0.003 m-thick layer of the ice section was removed with a stainless steel plane. The ice sample was then put in a polyethylene bag (Nihon Unipack Co., Ltd., Sapporo, Japan) and melted at room temperature (about 20°C). Snow samples were also melted at room temperature. The melting process was checked regularly. During the final melt phase, samples were swirled until the last pieces of ice or snow had melted to maintain the temperature at $\leq$0°C as much as possible throughout the melting process. Melted samples were handled and stored in the same manner as the crack water samples. For ice texture analysis, the second half of the ice core was sliced into 0.003 m-thick sections in the cold room (−16°C) at Hokkaido University, and the ice crystallographic structures were examined by illuminating the 0.003 m-thick sections between crossed polarizers (Langway, 1958).

The sections of the ice cores to be assayed for chl *a* were melted at room temperature with 300 mL of artificial seawater (40 g NaCl in 1 L Milli-Q water) to avoid the loss of intracellular organic solutes due to cell rupture caused by osmotic stress (Garrison & Buck, 1986). The melting process was checked regularly. During the final melt phase, samples were swirled until the last pieces of ice had melted to maintain the temperature at $\leq$0°C as much as possible throughout the melting process. Melted ice samples of known volume were filtered in the same manner as the crack water samples and then stored until analysis for chl *a*.

Salinity was measured on the Shirase with a salinity analyzer (SAT-210, Toa Electronics Ltd., Tokyo, Japan). The salinity analyzer was calibrated using International Association for the Physical Science of the Ocean standard seawater (P series; Ocean Scientific International Ltd., Hampshire, UK). The standard deviation for salinity, calculated from 15 subsamples taken from a reference water sample with water salinity of 10.00, was 0.03.

The $\delta^{18}O$ of water and melted ice core and snow samples was determined with a mass spectrometer (DELTA plus; Finnigan MAT, San Jose, CA) via the equilibration method. The $\delta^{18}O$ in per mil (‰) was calculated using the $^{18}O/^{16}O$ ratio of standard mean ocean water as the standard. The standard deviation of the $\delta^{18}O$, calculated from 10 subsamples taken from reference water with a $\delta^{18}O$ value of 0.241‰, was 0.026‰.

Chl *a* concentrations were determined on the Shirase within one month of sample collection. A fluorometer (Model 10AU, Turner Designs, Inc., Sunnyvale, CA) was used in accord with the method described by Parsons

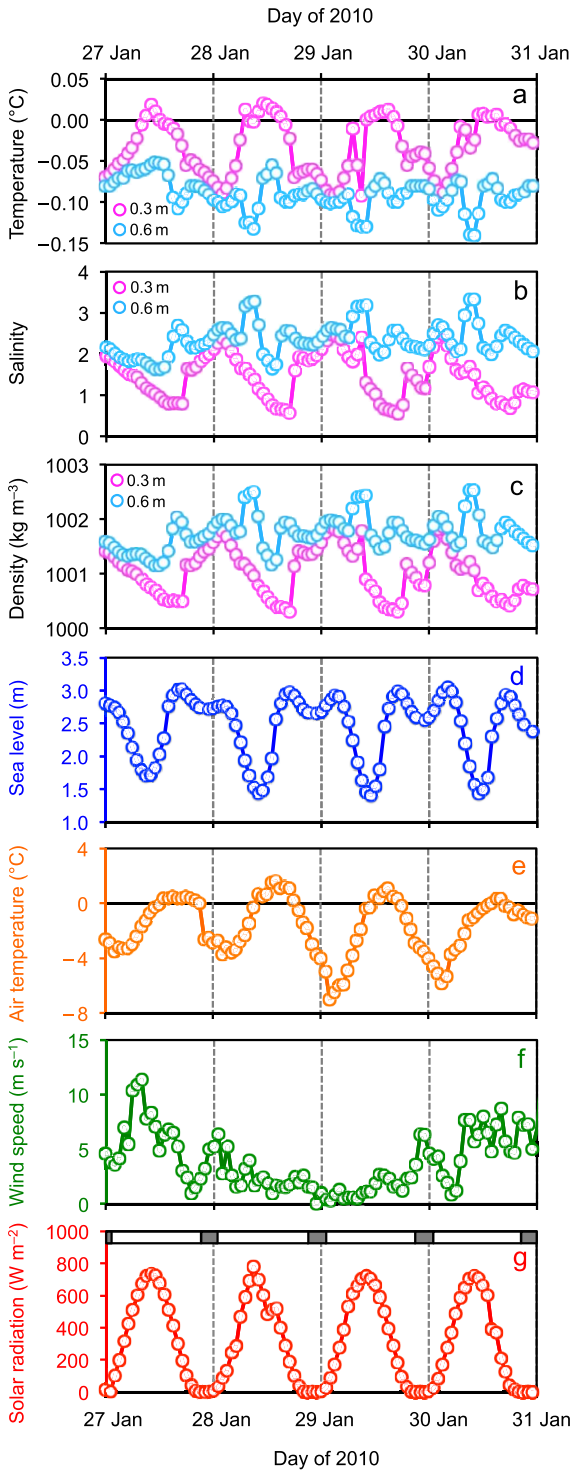

Figure 3. Time series of (a) sea ice crack-water temperature, (b) salinity, (c) density, (d) sea level, (e) air temperature, (f) wind speed, and (g) solar radiation. Temperature and salinity were obtained from the mooring experiment. Sea level (Japan Oceanographic Data Center; http://www.jodc.go.jp/index.html) and air temperature, wind speed, and solar radiation (Japan Meteorological Agency; http://www.data.jma.go.jp/obd/stats/etrn/index.php) were measured at Syowa Station, less than 1 km from our sea ice crack study area. The white and gray bars in Figure 3g indicate day and night, respectively.

et al. (1984). Standards (0.28–282.30 μg L^{-1} chl *a*) prepared from a liquid chl *a* standard (Wako Pure Chemical Industries Ltd., Osaka, Japan) by stepwise dilution with *N,N*-dimethylformamide were used to calibrate the fluorometer before chl *a* measurements. The algae in the water sample collected at C5 were examined under a microscope (Leica Microsystems, Germany) at 50–100X magnification. For species identification, we used Medlin and Priddle (1990) for the Southern Ocean algae. In this study, we simply estimated in qualitative terms whether the dominant algae were diatoms, and we checked whether the diatom frustules were broken or not.

The concentrations of nutrients ($NO_3^- + NO_2^-$, NH_4^+, and PO_4^{3-}) were determined at the Tokyo University of Marine Science and Technology within 6 months after sample collection. The assays were carried out using AutoAnalyzers: an AACS III (Bran + Luebbe, Tokyo, Japan) was used for dissolved inorganic nitrogen ($NO_3^- + NO_2^-$ and NH_4^+) and a Quaatro-Marine 5ch (SEAL Analytical, Ltd., Hampshire, UK) for PO_4^{3-}. The analytical procedures were in accord with the Joint Global Ocean Flux Study (JGOFS) spectrophotometric methods (Joint Global Ocean Flux Study, 1996). The standard deviations of the nutrient concentrations, calculated from 20 subsamples taken from reference water samples with $NO_3^- + NO_2^-$, NH_4^+, and PO_4^{3-} concentrations of 10.00, 9.99, and 2.11 μmol L^{-1} were 0.30, 0.18, and 0.06 μmol L^{-1}, respectively. Dissolved inorganic nitrogen (DIN) was equated to the sum of NO_3^-, NO_2^-, and NH_4^+.

The fractions of snow meltwater, sea ice meltwater, and under-ice seawater in the water samples were estimated on the basis of salinity and $\delta^{18}O$, both of which were assumed to be conservative. The fractions (*Fs*) were estimated from the following equations:

$$F_{snow} + F_{ice} + F_{sw} = 1 \quad (1)$$

$$F_{snow}S_{snow} + F_{ice}S_{ice} + F_{sw}S_{sw} = S_{sample} \quad (2)$$

$$F_{snow}\delta_{snow} + F_{ice}\delta_{ice} + F_{sw}\delta_{sw} = \delta_{sample} \quad (3)$$

where *S* and δ represent salinity and $\delta^{18}O$, respectively. The subscripts, "'*snow*," "*ice*," "*sw*," and "*sample*" refer to the snow meltwater, sea ice meltwater, under-ice seawater, and a water sample derived from crack water and slush, respectively. The fractions were then converted to percentages. The end-member value and standard deviation of the salinity and $\delta^{18}O$ for each source used in this study are listed in supporting information Table S2. For estimation of each fraction, end-member and water sample values were substituted into equations (2) and (3) and solved for each fraction. The calculated values varied by ±0.0% for S_{snow}, ±1.1% for δ_{snow}, ±1.1% for S_{ice}, ±10.1% for δ_{ice}, ±0.1% for S_{sw}, and ±0.1% for δ_{sw} when the end-member values were changed by one standard deviation.

3. Results

3.1. Sea Ice Crack Properties

The sea ice crack examined in this study was about 250 m long and formed in multiyear land-fast ice (3.2–4.0 m thick). The crack extended in an offshore direction from the northeast point of Ongul Island (Figure 1 and supporting information Table S1). The crack width ranged from 2 to 15 cm (supporting information Table S1), and overhead

photographs of the crack showed a strong brown color inside the crack (Figure 2a). Supporting information Table S3 shows the salinity, $\delta^{18}O$, chl *a*, and nutrient concentrations (DIN and PO_4^{3-}) of the crack water. The mean ± standard deviation of each parameter of the crack water was 1.3 ± 0.7 for salinity, −20.1 ± 1.2‰ for $\delta^{18}O$, 0.3 ± 0.3 μg L^{-1} for the chl *a* concentration, 1.3 ± 1.1 μmol L^{-1} for the DIN concentration, and 0.3 ± 0.2 μmol L^{-1} for the PO_4^{3-} concentration. Generally, concentrations of all constituents of the crack water were lower than those of the under-ice water, except for the chl *a* concentration, which was comparable to that of the under-ice water (supporting information Table S3). The fractions of snow meltwater, sea ice meltwater, and under-ice seawater in the crack water, estimated on the basis of salinity and $\delta^{18}O$, indicated that the crack water was composed of 64–84% snow meltwater, 12–30% sea ice meltwater, and 0–8% under-ice water. Microscopic examination of algal samples confirmed that the algae collected from the sea ice crack were diatoms. Most of the diatom frustules were broken.

Time series of crack water temperature, salinity, and density at depths of 0.3 and 0.6 m as well as sea level, air temperature, wind speed, and solar radiation are shown in Figure 3. Crack water temperature fluctuated from −0.14 to 0.02°C (Figure 3a). Salinity varied from 0.6 to 3.3, which is low compared to that of seawater (supporting information Table S3). The correlation between temperature and salinity was significant and negative ($n = 564$, $r^2 = 0.92$, $p < 0.001$). The temperature generally increased and salinity decreased during the daytime, and temperature decreased and salinity increased at night (Figures 3a and 3b). Variations of crack water temperature at 0.3 m were synchronous with fluctuations in solar radiation and air temperature (Figures 3a, 3e, and 3g). Temperature and salinity followed similar diurnal patterns at depths of 0.3 and 0.6 m, but the magnitudes of the diurnal variations were much lower at 0.6 m than at 0.3 m. In addition, changes toward lower temperatures and higher salinities in the forenoons of 28–30 January resulted in distinct semidiurnal cycles. The variations of temperature and salinity at 0.6 m therefore reflected the influence of deeper water, as evidenced by variations in sea level (Figures 3a–3g).

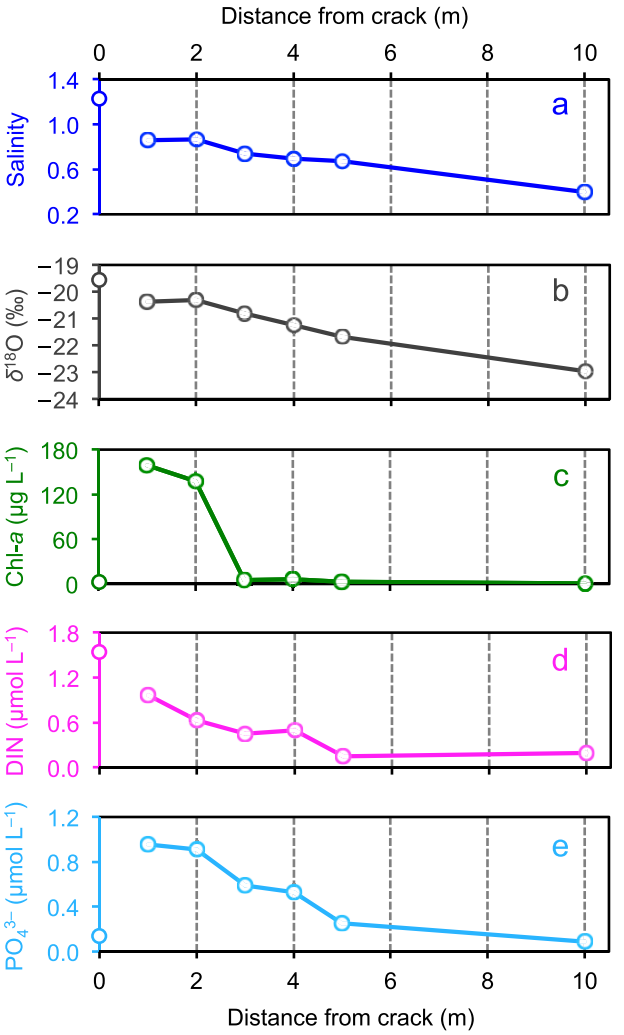

Figure 4. Horizontal distribution of (a) salinity, (b) $\delta^{18}O$, (c) chl *a* concentration, (d) DIN concentration, and (e) PO_4^{3-} concentration for the water in the slush layer through point S1–10 at station C5.

3.2. Slush Layer Properties

The slush layer depth ranged from 0.06 to 0.16 m (supporting information Table S1). Overhead photographs of the slush water layer showed that the intensity of the discoloration (brown color) in the slush layer diminished as the distance from the crack increased (Figure 2a). Figure 4 shows the horizontal distribution of salinity, $\delta^{18}O$, chl *a*, and nutrient concentrations (DIN and PO_4^{3-}) of slush water at points S1–10. With increasing distance from the edge of the crack, salinity, $\delta^{18}O$, chl *a*, and nutrient concentrations (DIN and PO_4^{3-}) of the slush water decreased (Figure 4 and supporting information Table S3). Slush water at M1 was characterized by a relatively high $\delta^{18}O$, low chl *a* concentration, and salinity and nutrient concentrations that were similar to those at points S1–10 (supporting information Table S3). Similar to the crack water, concentrations of all constituents of the slush water were generally lower than those of the under-ice water, except for the chl *a* concentrations (supporting information Table S3). The chl *a* concentrations in the slush water at S1 and S2 were relatively high (138–159 μg L^{-1}; Figure 4c and supporting information Table S3). The fraction of snow meltwater estimated on the basis of salinity and $\delta^{18}O$ increased from 75 to 85% with increasing distance from the edge of the crack, while the fractions of sea ice meltwater and under-ice water decreased from 25% to 10% and from 2% to 1%, respectively (Figure 5).

3.3. Sea Ice and Snow Properties

Figure 6 shows depth profiles of salinity, $\delta^{18}O$, chl *a*, and nutrient concentrations (DIN and PO_4^{3-}) of the sea ice at C7 (Figures 6a–6e) and M1

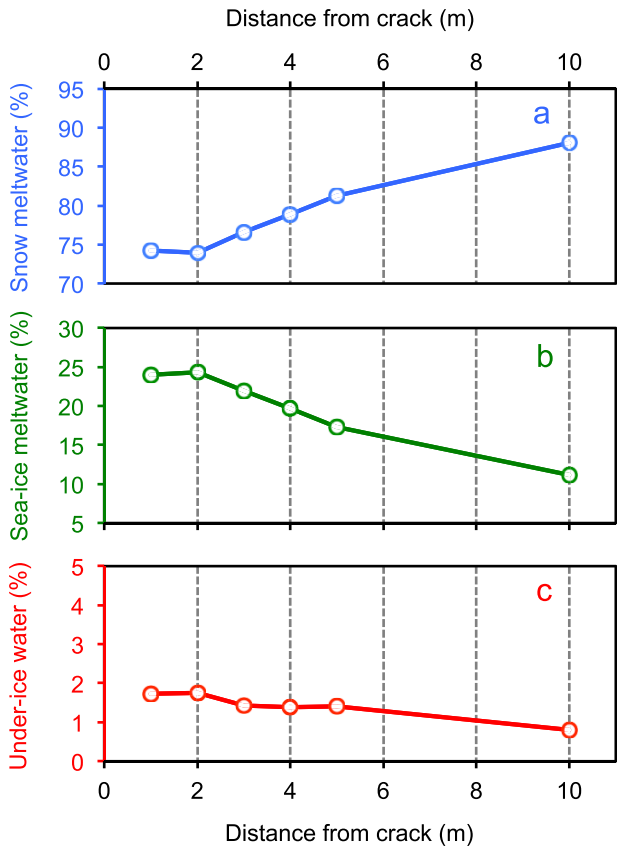

Figure 5. Horizontal distribution of (a) the percentages of the snow-melt water, (b) sea ice meltwater, and (c) under-ice water for the water in the slush layer through point S1–10 at station C5.

(Figures 6g–6k); values of snow and slush are also indicated. The salinity was zero in the snow and increased slightly in the slush layer at both sites (Figures 6a and 6g). The salinity of the sea ice varied from 0 to 4. The $\delta^{18}O$ of snow was identical at both sites and equaled $-24.1 \pm 1.0‰$ (mean $\pm$ standard deviation). Most of the sea ice $\delta^{18}O$ values were negative at C7, whereas at M1 they were zero, except for the top 0.2 m of the sea ice (Figures 6b and 6h). There were peaks of chl *a* concentrations up to 5.4 $\mu g\ L^{-1}$ in the top, middle, and bottom of the sea ice at C7 (Figure 6c). In contrast, there were two peaks of chl *a* concentrations in the bottom part of the sea ice at M1 (Figure 6i). The concentrations of DIN and PO_4^{3-} were zero in the snow at both sites, but they increased in the slush and sea ice (Figures 6d, 6e, 6j, and 6k). At C7, there were some nutrient concentration peaks within the sea ice (19.8 $\mu mol\ L^{-1}$ for the DIN concentration and 1.5 $\mu mol\ L^{-1}$ for the PO_4^{3-} concentration). However, at M1, the DIN concentrations were uniformly low throughout the sea ice, and a peak of PO_4^{3-} occurred only at the bottom of the sea ice (Figures 6j and 6k). One of the peaks of salinity, chl *a*, DIN, and PO_4^{3-} at C7 corresponded to the discoloration (brown color) in the middle of the sea ice (Figures 6a, 6c, 6d, and 6e).

Analysis of the sea ice texture at C7 indicated that granular ice (snow ice plus frazil ice) dominated most of the ice core samples (87% of total ice thickness); columnar ice in the bottom part of the sea ice accounted for the remaining 13% of the total ice thickness (Figure 6f). In contrast, columnar ice dominated most of the ice core samples at M1 (90% of total ice thickness), and granular ice in the top part of the sea ice accounted for 10% of the total ice thickness (Figure 6l).

3.4. Relationship Between Salinity and Nutrient Concentration

We plotted salinity and nutrient concentrations (DIN and PO_4^{3-}) in crack water, slush water, snow, and sea ice and compared the results with the theoretical dilution line based on the values of the under-ice water (Figure 7). Most nutrient concentrations in the sea ice at C7 (96% of the samples) were higher than predicted by the dilution line for both DIN and PO_4^{3-}. In contrast, sea ice nutrient concentrations at M1 were equal to or less than values predicted by the dilution line, the indication being that there had been no net enrichment or net uptake of both DIN and PO_4^{3-}. Crack and slush nutrient concentrations were close to values predicted by the dilution line in the case of DIN (Figure 7a), but higher in the case of PO_4^{3-} (Figure 7b).

4. Discussion

4.1. Genesis of Sea Ice Crack in the Sampling Area

The sea ice crack examined in this study extended offshore from the edge of the Ongul Islands (Figure 1). This kind of crack forms almost every year in this multiyear ice area during the spring and summer (G. Hashida, wintering team leader at Syowa Station between 2012 and 2014, personal communication). A strong contrast in ice thickness develops during the ice melt season between two areas of the Ongul Strait. The area located between the Ongul Islands and the Antarctic continent experiences little snow accumulation, being downwind of the continent and icebergs (dark gray area of sea ice in Figure 1). As a result, the sea ice surface consists of bare ice and surface ponds, and sea ice thickness is typically $<$1.5 m (Nomura et al., 2011a) at the start of the melt season when bottom melting begins. In contrast, the ice in the area on the other side of the strait (light gray area of sea ice in Figure 1) is much thicker ($>$3 m) and is covered with snow and influenced by snow ice formation. In addition, the presence of the Ongul Islands restricts the horizontal movement of the sea ice and thereby generates stress. This stress leads to a fracture at the interface between the thick and thin ice, and a bending crack is formed as a result.

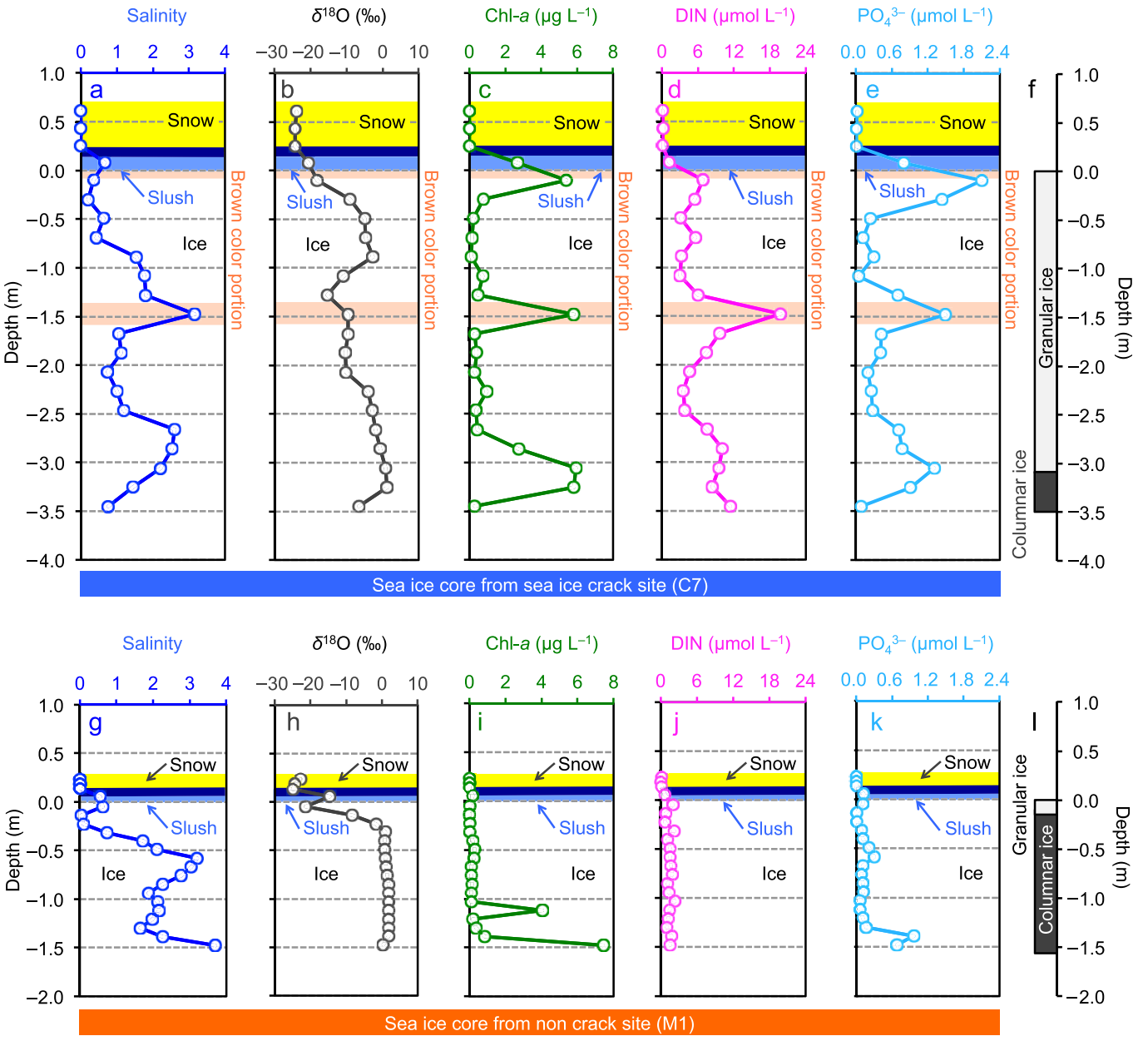

Figure 6. Depth profiles of (a, g) salinity, (b, h) $\delta^{18}O$, (c, i) chl *a* concentration, (d, j) DIN concentration, (e, k) PO_4^{3-} concentration, and (f, l) sea ice structure at (a–f) C7 and (g–l) M1. The yellow, blue, light blue, and brown shading (Figures 6a–6e and 6g–6k) indicate the snow, superimposed ice, slush, and discoloration (brown) portions of the sea ice, respectively.

4.2. Biological Productivity Within the Sea Ice Crack

The inside of the crack was characterized by an intense discoloration (brown color) (Figure 2a) during the observation period, the suggestion being that there was at some point high biological productivity within the crack water. The particulate matter formed as a result of the previous biological productivity in the crack water presumably sank after the bloom and became attached to the side of the crack, where the organic matter was remineralized. Microscopic examination of the algal samples supported this remineralization scenario, because most of the diatom frustules were broken. The fact that most DIN and all PO_4^{3-} concentrations in the crack water were higher than predicted by the dilution line (Figure 7) also supports the remineralization scenario (Fripiat et al., 2014; Thomas et al., 1995).

The abrupt opening of cracks allows sunlight to directly enter the surface water. Algal blooms then occur within the crack water. The results of a previous artificial pool experiment near the crack site at the same

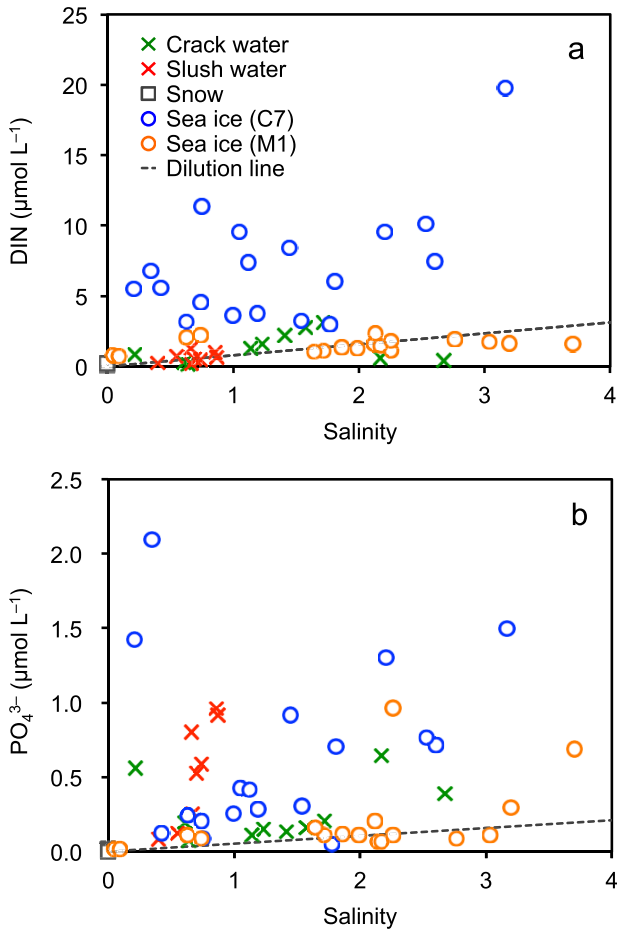

Figure 7. Plots of concentrations of (a) DIN and (b) PO_4^{3-} versus salinity in crack water, slush water, snow, and sea ice. The dashed lines indicate dilution lines, which connected the origin (zero) and the points corresponding to under-ice water for salinity and nutrient concentrations.

time of year (Nomura et al., 2012b) facilitate discussion of the relationships between algal blooms and the physicochemical environment. During that experiment, an algal bloom occurred almost one month after opening of the artificial pool surface (1.5 m × 1.5 m). Stratification and stability of the water column were important conditions for the onset of the bloom. At the end of the experiment, the surface water became brown (chl *a*: 4 μg L^{-1}). At the same time, the nutrient concentrations in the pool water decreased owing to a combination of biological uptake and dilution by freshwater from snow and ice (Nomura et al., 2012b). In this study, salinity-$\delta^{18}O$ measurements confirmed that 64–84% of the crack water consisted of snow meltwater that was produced during the melt season. In addition, the influx of freshwater from melting and heat from solar radiation caused the crack water to freshen and warm. The result was stratification of the crack water (Figure 6), which created conditions favorable for algal growth (Nomura et al., 2012b). Our results suggest that formation of sea ice cracks creates conditions favorable for biological productivity by adding freshwater and abruptly increasing the influx of sunlight to the surface water. The result is formation of a stratified water column with light and nutrient concentrations sufficient to trigger an algal bloom. The subsequent decrease of nutrient concentrations due to biological uptake and stratification of the water column due to freshwater inputs to the semi-enclosed environment of the crack limited the magnitude and duration of the bloom, although the tidal cycle provided an opportunity for nutrients to be added from the underlying seawater to the inside of the crack. In addition, the combined effects of algal mortality, light inhibition, and osmotic stress on the algal cells (e.g., Garrison & Buck, 1986) would have limited the magnitude and duration of the bloom.

A mooring experiment indicated that the temperature at a depth of 0.3 m changed in phase with solar radiation and air temperature (Figures 3a, 3e, and 3g). The temperature monitored at 0.3 m exceeded 0°C in the daytime (Figure 3a), an indication that short-wave radiation and/or sensible heat flux caused warming of the crack water. Salinity in the crack increased as the temperature decreased, but it did not increase monotonically because of the supply of freshwater from above (Figures 3a and 3b). There were spikes of relatively high and low salinity and temperature, respectively, at a depth of 0.6 m during the mornings of 28–30 January. The times of the spikes coincided with times of rapid decreases of sea level (Figure 3d). Although there were no direct measurements of tidal currents, the tidal current is generally strong when sea level is changing rapidly. It is therefore very likely that the increase of the tidal current below the fast ice enhanced the exchange of water between the crack and seawater underneath, the result being an increase of the salinity of the crack water. During the night, the combined effects of heat loss to the atmosphere, the absence of warming and melting by sunlight, and mixing and sinking of the surface water by cooling caused the temperature and salinity at depths of 0.3 and 0.6 m to approach each other (Figures 3a and 3b), and hence the densities at these depths became similar (Figure 3c). The weakened stratification led to enhanced mixing of the water within the upper part of the crack and inside the slush layer.

Another factor contributing to the increase of salinity might have been ice formation and concomitant brine rejection. However, a simple salt budget calculation suggested that ice formation was an unlikely explanation for the increase of salinity. For example, salinity increased from 0.5 in the afternoon to 2.5 at night within the top 0.3 m of the crack water (Figure 3b). To increase the salinity by 2 within 0.3 m of the water column would have required 0.24 m of pure ice to form within the crack. However, we observed very thin (about 0.01 m) refrozen surface ice in the crack during the observation period. Our results therefore suggest that water exchange during the tidal cycle was the driving force that supplied seawater through the crack to the slush layer that developed over the sea ice.

4.3. Dynamics of Sea Ice Growth

When sufficient snow had been deposited on the sea ice, the ice surface was depressed below sea level and flooded. A slush layer therefore formed at the interface between the snow and sea ice (Ackley et al., 2008; Eicken et al., 1994; Haas et al., 2001; Jeffries et al., 2001; Jutras et al., 2016; Lange et al., 1990). Subsequent freezing of the slush layer led to the formation of snow ice (Kawamura et al., 1997; Maksym & Jeffries, 2000).

In this study, analysis of sea ice texture indicated that granular ice dominated most of the sea ice column, and the δ^{18}O values of the granular ice were negative at C7 (Figures 6b and 6f). These results indicate that the sea ice collected at the crack site (C7) was affected mainly by formation of snow ice. In a previous study that examined snow ice at a deep snow site in the same area (Kawamura et al., 1997), the δ^{18}O of the sea ice surface (about $-20‰$) was identical to our values, a result consistent with snow-ice formation in this study. At M1, where the rate of snow accumulation was low in the land-fast ice compared to the rate at C7 (supporting information Table S1 and Figure 1), granular ice with negative δ^{18}O values was found only at the top of the sea ice (Figures 6h and 6l), the indication being that the contribution of snow to sea ice growth was insignificant.

4.4. Formation of the Slush Layer and Water Supply

During the formation of a slush layer, water is supplied to the layer by horizontal movement from the edge of the ice floe and through upward percolation of seawater through permeable sea ice (Golden et al., 1998; Haas et al., 2001; Perovich et al., 2004) where the sea ice is fractured.

Here we discuss the possibility of upward percolation of seawater from the bottom of the ice through the brine channel. The brine volume fraction is a useful parameter for assessing the likelihood of upward percolation of seawater through sea ice. The temperature and salinity of the sea ice were used to calculate the brine volume fraction. However, at C7, we could not obtain realistic ice temperature data because of the difficulty of making a hole to insert a temperature sensor in the sea ice. When the hole was being drilled, the ice temperature increased because of the friction between the drill bit and the ice. The ice was very hard where its salinity was low ($S < 1$) near the surface of multiyear ice (Figure 6a). We assumed that the temperature of the ice was -1.8°C throughout the ice column, an assumption that leads to a maximum estimate for the brine volume. The brine volume fraction of the sea ice at C7, calculated according to Leppäranta and Manninen (1988), was low, with a mean of 3.3% (range: 0.5–7.8%). Therefore, upward percolation of seawater was more-or-less inhibited when the brine volume fraction was less than 5.0–7.5% because of the reduced permeability of the sea ice (Golden et al., 1998; Pringle et al., 2009; Zhou et al., 2013). In fact, salinity-δ^{18}O measurements of slush water confirmed that only 1–2% of the slush water consisted of under-ice water (Figure 5c). These results suggest that the potential for upward percolation of seawater from the bottom of the ice through the >3 m-thick, multiyear ice was minimal.

The horizontal gradients of salinity and δ^{18}O within the slush water revealed that the water from the crack was advected into the sea ice (Figures 4a and 4b). When the crack formed in the sea ice, seawater from beneath the sea ice was transported to the surface within the crack. Surface seawater in the crack was then advected and incorporated into the slush layer. During this process, meltwater from snow and sea ice was added to the crack and slush layer. The salinity and concentrations of biogeochemical constituents were therefore decreased by dilution and became lower in the slush water than in the under-ice water (supporting information Table S3). In fact, salinity-δ^{18}O measurements for slush water confirmed that 75% and 25% of slush water consisted of snow meltwater and sea ice meltwater, respectively (Figure 5).

4.5. Influence of Sea Ice Crack Formation on the Spatial Distribution of Microalgae in the Slush Layer and Sea Ice

In the case of the chl *a* concentrations, however, we observed much higher concentrations (137.5–159.2 $\mu g\ L^{-1}$) in the slush water near the crack (S1 and S2; Figures 2a and 4c and supporting information Table S3) than at the other positions and stations (0.2–6.6 $\mu g\ L^{-1}$ at S3–10 and M1), and during a previous study in the Weddell Sea in December (2004) in the slush water on a 100 km^2 ice floe with no crack near the slush layer (0.4–44.7 $\mu g\ L^{-1}$; Papadimitriou et al., 2009). Nutrients were supplied when crack water, driven by the tidal cycle, penetrated from the edge of the crack into the slush layer at the initial stage of crack formation and algal growth.

For the other positions and station (S3–10 and M1), there was less influence from the crack because S3–10 and M1 were located much further from the crack than S1 and S2. The salinity and concentrations of biogeochemical constituents of the slush water were lower at S3–10 and M1 than at S1 and S2 (Figure 4 and supporting information Table S3) because of dilution of all slush water parameters, including nutrients. We calculated the quantity of nutrients required to support the observed chl *a* concentration of 159 μg L^{-1} at S1 as an example. For the calculation, we assumed a carbon (as particulate organic carbon: POC):chl *a* ratio of 242 (g:g), which has been reported for the pack ice of the Ross Sea, Antarctica during springtime (Arrigo et al., 2003). The amount of DIN required to produce the POC was then calculated using a Redfield C:N ratio (mol:mol) of 6.6. The results indicated that 486 μmol of DIN were required to produce the observed chl *a* concentrations in 1 L of the slush water at S1. This value was much higher than the DIN concentration in the crack water (0.1–2.8 μmol L^{-1}) and the under-ice water (21.6–27.2 μmol L^{-1}) observed in this study (supporting information Table S3). Therefore, tidal resupply of nutrients to the slush layer was needed to support the observed chl *a* concentrations.

The irradiance within the slush layer below the snow cover is obviously an important constraint on primary production within the slush layer. Odate et al. (2004) have examined the attenuation of light through the snow and sea ice near Syowa Station, Antarctica, a location within our study area. Results indicated that snow reduced the irradiance to about 20% of the surface irradiance (Odate et al., 2004). Hence, the irradiance within the slush layer would have been enough for algal growth during the summer and well above the irradiance associated with the bottom of the euphotic zone, 0.1–1% of the surface irradiance. It is believed that microalgae in sea ice are adapted to low irradiance (Arrigo, 2003). Therefore, in this study the ice algae were probably shade adapted, and the irradiance should have been adequate for photosynthesis, although snow has a high albedo (Perovich & Polashenski, 2012).

Our results therefore indicate that sea ice crack formation can be critical for the occurrence of algal blooms, not only in the cracks themselves but also in the surrounding sea ice environment. In the case of factors determining the growth of algae within slush water, the frequency of crack formation and the spatial distribution of the cracks would also be important.

Biogeochemical constituents transported from the crack into the slush layer were preserved in the sea ice through formation of snow ice at the edge of the crack, where the snow depth was relatively high (supporting information Table S1 and Figure 6). There were some peaks of chl *a* and nutrient concentrations (DIN and PO_4^{3-}) at the top, middle, and bottom of the sea ice layer in the ice core collected at C7 (Figures 6c–6e). These peaks corresponded to peaks in the intensity of the discoloration of the sea ice, except at the bottom of the sea ice layer (Figure 6). Our results therefore suggest that sea ice crack formation resulted in the transport of biogeochemical constituents into the slush layer, and from the slush layer they were preserved in the upper part of the sea ice during snow-ice formation. It is important to note that the sea ice examined in this study was multiyear ice. The biogeochemical constituents preserved in the sea ice would therefore provide information about the history of ice growth and the environmental conditions when slush water was incorporated into the surface of the sea ice, although meltwater from snow and sea ice would decrease the nutrient and chl *a* concentrations.

During the storage of biogeochemical constituents within sea ice, biological activity modified the status of the biogeochemical constituents. The organic matter that formed as a result of biological production in the crack and in the slush via in situ growth was transported into the slush layer and then preserved in the sea ice during the formation of snow ice. During photosynthesis, algal uptake decreased the concentrations of dissolved nutrients in the sea ice (e.g., Gleitz et al., 1995). Subsequently, remineralization of organic matter by heterotrophic organisms increased the nutrient concentrations in the sea ice (Thomas et al., 1995). The effects of these processes were most apparent in the highly productive parts of the sea ice, where the concentration of particulate organic compounds was high. In this study, we found peaks of the chl *a* and nutrient concentrations (DIN and PO_4^{3-}) in the top, middle, and bottom of the layer of sea ice at C7 (Figures 6c–6e). Therefore, both photosynthesis and remineralization occurred in those parts of the sea ice. Throughout the sea ice column at C7, the positive offsets of the nutrient concentrations from the dilution line suggested that remineralization rates exceeded photosynthetic rates (Figure 7). The thick accumulation of snow over the sea ice (supporting information Table S1) and the formation of ice from snow at the bottom of the snow layer created light-limited conditions (Ehn et al., 2008). It is therefore reasonable to conclude that remineralization exceeded photosynthesis within the sea ice at C7.

Several studies have indicated that atmospheric transfer and deposition of nutrients onto sea ice is an important source of nutrients for the potentially nutrient-depleted surfaces of sea ice (Granskog et al., 2003; Granskog & Kaartokallio, 2004; Krell et al., 2003; Nomura et al., 2011b). In the Northern Hemisphere, snow on sea ice contains especially high concentrations of nutrients, which are incorporated into the ice during formation of snow ice. In the case of Antarctica, atmospheric deposition of nutrients is minimal because of the relative cleanliness of the air and precipitation. Therefore, the flooding of water through the brine channel network close to the ice edge and within an individual ice floe is a key process that supplies nutrients to the sea ice surface (Ackley et al., 2008). For multiyear land-fast ice, the supply of water through the brine channel and edge of the ice is constrained by the thickness of the low-salinity ice (low brine volume fraction) and the stability of the ice (i.e., absence of fractures). Therefore, formation of cracks in the sea ice in the area of multiyear land-fast ice provides biogeochemical constituents to the upper part of the sea ice. This process has a strong impact on the supply of nutrients to the generally nutrient-depleted surfaces of sea ice (McMinn et al., 1999; Nomura et al., 2011a).

5. Concluding Remarks

Our results clearly indicate that formation of cracks in sea ice affects the environment where biological production and biogeochemical cycling occur in the surface ocean of sea ice systems. Because cracks are likely to form frequently within the sea ice during the season of ice melting and ice breaking, the contributions of cracks to biological production and biogeochemical cycling may be significant in ice-covered oceans. However, it is difficult to quantify the number of cracks over a wider area because the resolution of satellite images is too low to identify the cracks. In addition, snow cover on sea ice cracks restricts visual observations. Therefore, so far, it is difficult to clear up how much cracks near bloom would contribute to large-scale patterns.

Acknowledgments
We express our heartfelt thanks to H. Shinagawa, S. Chavanich, H. Shimoda, S. Koga, S. Youkongkaew, and all of the members of 51st Japanese Antarctic Research Expedition for their support in the fieldwork. We thank M. Kitagawa for the oxygen isotopic ratio analyses, C. Oouchida, S. Yasui, and J. Kanda for their nutrient analyses, and D. H. Han for microscopic examination of the algae sample. This research was supported by funds from the National Institute of Polar Research and the Japan Society for the Promotion of Science (grants 21810036 and 25281001, respectively). Data for the physicochemical parameters used in this study are shown in supporting information Tables S1–S3. Sea level, air temperature, wind speed, and solar radiation are cited at http://www.jodc.go.jp/index.html (Japan Oceanographic Data Center) and http://www.data.jma.go.jp/obd/stats/etrn/index.php (Japan Meteorological Agency).

References

Ackley, S. F., Lewis, M. J., Fritsen, C. H., & Xie, H. (2008). Internal melting in Antarctic sea ice: Development of "gap layers." *Geophysical Research Letters*, *35*, L11503. https://doi.org/10.1029/2008GL033644

Ackley, S. F., & Sullivan, C. W. (1994). Physical controls on the development and characteristics of Antarctic sea ice biological communities—A review and synthesis. *Deep Sea Research Part I: Oceanographic Research Papers*, *41*, 1583–1604.

Arrigo, K. R. (2003). Primary production in sea ice. In D. N. Thomas & G. S. Dieckmann (Eds.), *Sea ice—An introduction to its physics, chemistry, biology and geology* (pp. 143–183). Oxford, UK: Blackwell Science.

Arrigo, K. R., Robinson, D. H., Dunbar, R. B., Leventer, A. R., & Lizotte, M. P. (2003). Physical control of chlorophyll *a*, POC, and TPN distributions in the pack ice of the Ross Sea, Antarctica. *Journal of Geophysical Research: Oceans*, *108*(C10), 3316. https://doi.org/10.1029/2001JC001138

Ehn, J. K., Munday, C. J., & Barber, D. G. (2008). Bio-optical and structural properties inferred from irradiance measurements within the bottommost layers in an Arctic Landfast sea ice cover. *Journal of Geophysical Research: Oceans*, *113*, C03S03. https://doi.org/10.1029/2007JC004194

Eicken, H., Lange, M. A., Hubberten, H.-W., & Wadhams, P. (1994). Characteristics and distribution patterns of snow and meteoric ice in the Weddell Sea and their contribution to the mass balance of sea ice. *Annals of Geophysics*, *12*, 80–93.

Fripiat, F., Sigman, D. M., Fawcett, S. E., Rafter, P. A., Weigand, M. A., & Tison, J.-L. (2014). New insights into sea ice nitrogen biogeochemical dynamics from the nitrogen isotopes. *Global Biogeochemical Cycles*, *28*, 115–130. https://doi.org/10.1002/2013GB004729

Fritsen, C. H., Lytle, V. I., Ackley, S. F., & Sullivan, C. W. (1994). Autumn bloom of Antarctic pack-ice algae. *Science*, *266*, 782–784.

Garrison, D. L., & Buck, K. R. (1986). Organism losses during ice melting: A serious bias in sea ice community studies. *Polar Biology*, *6*, 237–239.

Gleitz, M., Vonderlo, M. R., Tomas, D. N., Dieckmann, G. S., & Millero, F. J. (1995). Comparison of summer and winter inorganic carbon, oxygen and nutrient concentrations in Antarctic sea ice brine. *Marine Chemistry*, *51*, 81–89.

Golden, K. M., Ackley, S. F., & Lytle, V. I. (1998). The percolation phase transition in sea ice. *Science*, *282*, 2238–2241.

Granskog, M. A., & Kaartokallio, H. (2004). An estimation of the potential fluxes of nitrogen, phosphorus, cadmium and lead from sea ice and snow in the northern Baltic Sea. *Water, Air, & Soil Pollution*, *154*, 331–347.

Granskog, M. A., Kaartokallio, H., & Shirasawa, K. (2003). Nutrient status of Baltic Sea ice: Evidence for control by snow-ice formation, ice permeability, and ice algae. *Journal of Geophysical Research: Oceans*, *108*(C8), 3253. https://doi.org/10.1029/2002JC001386

Haas, C., Thomas, D. N., & Bareiss, J. (2001). Surface properties and processes of perennial Antarctic sea ice in summer. *Journal of Glaciology*, *47*(159), 613–625.

Higashi, A., Goodman, D. J., Kawaguchi, S., & Mae, S. (1982). The cause of the breakup of fast ice on March 18, 1980 near Syowa station, East Antarctica. *Memoirs of National Institute of Polar Research*, *24*, 222–231.

Jeffries, M. O., Krouse, H. R., Hurst-Cushing, B., & Maksym, T. (2001). Snow-ice accretion and snow-cover depletion on Antarctic first-year sea-ice floes. *Annals of Glaciology*, *33*, 51–60.

Joint Global Ocean Flux Study. (1996). *Protocols for the Joint Global Ocean Flux Study core measurements* (JGOFS Rep. 19). Bergen, Norway: Centre for Studies of Environment and Resources. JGOFS Core Project Office.

Jutras, M., Vancoppenolle, M., Lourenço, A., Vivier, F., Carnat, G., Madec, G., et al. (2016). Thermodynamics of slush and snow–ice formation in the Antarctic sea-ice zone. *Deep Sea Research Part II: Topical Studies in Oceanography*, *131*, 75–83.

Kattner, G., Thomas, D. N., Haas, C., Kennedy, H., & Dieckmann, G. S. (2004). Surface ice and gap layers in Antarctic sea ice: Highly productive habitats. *Marine Ecology Progress Series*, *277*, 1–12.

Kawamura, T., Ohshima, K. I., Takizawa, T., & Ushio, S. (1997). Physical, structural, and isotopic characteristics and growth processes of fast sea ice in Lützow-Holm Bay, Antarctica. *Journal of Geophysical Research: Oceans*, *102*(C2), 3345–3355.

Krell, A., Ummenhofer, C., Kattner, G., Naumov, A., Evans, D., Dieckmann, G. S., et al. (2003). The biology and chemistry of land fast ice in the White Sea, Russia—A comparison of winter and spring conditions. *Polar Biology*, *26*, 707–719.
Lange, M. A., Schlosser, P., Ackley, S. F., Wadhams, P., & Dieckmann, G. S. (1990). ^{18}O concentrations in sea ice of the Weddell Sea, Antarctica. *Journal of Glaciology*, *36*(124), 315–323.
Langway, C. C. (1958). *Ice fabrics and the universal stage* (Rep. 62). U.S. Army Corps of Engineers, Snow, Ice and Permafrost Research Establishment.
Leppäranta, M., & Manninen, T. (1988). *The brine and gas content of sea ice with attention to low salinities and high temperatures* (Internal Rep. 88-2). Helsinki, Finland: Finnish Institute of Marine Research.
Loose, B., McGillis, W. R., Perovich, D., Zappa, C. J., & Schlosser, P. (2014). A parameter model of gas exchange for the seasonal sea ice zone. *Ocean Science*, *10*(1), 17–28.
Maksym, T., & Jeffries, M. O. (2000). A one-dimensional percolation model of flooding and snow-ice formation on Antarctic sea ice. *Journal of Geophysical Research: Oceans*, *105*(C11), 26313–26331.
Maykut, G. A. (1978). Energy exchange over young sea ice in the central Arctic. *Journal of Geophysical Research: Oceans*, *83*(C7), 3646–3658.
McMinn, A., Skerratt, J., Trull, T., Ashworth, C., & Lizotte, M. (1999). Nutrient stress gradient in the bottom 5 cm of fast ice, McMurdo Sound, Antarctica. *Polar Biology*, *21*, 220–227.
Medlin, L. K., & Priddle, J. (1990). *Polar marine diatoms*. Cambridge, UK: British Antarctic Survey, Natural Environment Research Council.
Moore, C. W., Obrist, D., Steffen, A., & Staebler, R. M. (2014). Convective forcing of mercury and ozone in the Arctic boundary layer induced by leads in sea ice. *Nature*, *506*, 81–84.
Nomura, D., Granskog, M. A., Assmy, P., Simizu, D., & Hashida, G. (2013). Arctic and Antarctic sea ice acts as a sink for atmospheric CO_2 during periods of snowmelt and surface flooding. *Journal of Geophysical Research: Oceans*, *118*, 6511–6524. https://doi.org/10.1002/2013JC009048
Nomura, D., Koga, S., Kasamatsu, N., Shinagawa, H., Simizu, D., Wada, M., et al. (2012a). Direct measurements of DMS flux from Antarctic fast sea ice to the atmosphere by a chamber technique. *Journal of Geophysical Research: Oceans*, *117*, C04011. https://doi.org/10.1029/2010JC006755
Nomura, D., McMinn, A., Hattori, H., Aoki, S., & Fukuchi, M. (2011b). Incorporation of nitrogen compounds into sea ice from atmospheric deposition. *Marine Chemistry*, *127*, 90–99.
Nomura, D., Simizu, D., Chavanich, S., Shinagawa, H., & Fukuchi, M. (2012b). An artificial pool experiment in Antarctic sea ice: Effects of sea-ice melting on physical and biogeochemical components of pool water. *Antarctic Science*, *24*(5), 536–544. https://doi.org/10.1017/S0954102012000284
Nomura, D., Simizu, D., Shinagawa, H., Oouchida, C., & Fukuchi, M. (2011a). Biogeochemical properties of water in surface ponds on Antarctic fast ice and relationship to underlying sea ice properties. *Journal of Glaciology*, *57*(205), 1–9.
Odate, T., Hirawake, T., & Fukuchi, M. (2004). Empirical relationship between sea ice thickness and underwater light intensity based on observations near Syowa Station, Antarctica, in austral summer. *Antarctic Record*, *48*(2), 91–97.
Papadimitriou, S., Thomas, D. N., Kennedy, H., Kuosa, H., & Dieckmann, G. S. (2009). Inorganic carbon removal and isotopic enrichment in Antarctic sea ice gap layers during early austral summer. *Marine Ecology Progress Series*, *386*, 15–27.
Parsons, T. R., Takahashi, M., & Hargrave, B. (1984). *Biological oceanographic processes* (3rd ed., 330 pp.). Oxford, UK: Pergamon.
Perovich, D. K., Elder, B. C., Claffey, K. J., Stammerjohn, S. E., Smith, R. C., Ackley, S. F., et al. (2004). Winter sea-ice properties in Marguerite Bay, Antarctica. *Deep Sea Research Part II: Topical Studies in Oceanography*, *51B*, 2023–2039.
Perovich, D. K., & Polashenski, C. (2012). Albedo evolution of seasonal Arctic sea ice. *Geophysical Research Letters*, *39*, L08501. https://doi.org/10.1029/2012GL051432
Petrich, C., Langhorne, P. J., & Haskell, T. G. (2007). Formation and structure of refrozen cracks in land-fast first-year sea ice. *Journal of Geophysical Research: Oceans*, *112*, C04006. https://doi.org/10.1029/2006JC003466
Pringle, D. J., Miner, J. E., Eicken, H., & Golden, K. M. (2009). Pore space percolation in sea ice single crystals. *Journal of Geophysical Research: Oceans*, *114*, C12017. https://doi.org/10.1029/2008JC005145
Schnack-Schiel, B., Thomas, D. N., Haas, C., Dieckmann, G. S., & Alheit, R. (2001). The occurrence of the copepods *Stephos longipes* (Calanoida) and *Drescheriella glacialis* (Harpacticoida) in summer sea ice in the Weddell Sea, Antarctica. *Antarctic Science*, *13*(2), 150–157.
Steiner, N. S., Lee, W. G., & Christian, J. R. (2013). Enhanced gas fluxes in small sea ice leads and cracks: Effects on CO_2 exchange and ocean acidification. *Journal of Geophysical Research: Oceans*, *118*, 1195–1205. https://doi.org/10.1002/jgrc.20100
Suzuki, R., & Ishimaru, T. (1990). An improved method for the determination of phytoplankton chlorophyll using *N*,*N*-dimethylformamide. *Journal of the Oceanographic Society of Japan*, *46*, 190–194. https://doi.org/10.1007/BF02125580
Thomas, D. N., Lara, R. J., Eicken, H., Kattner, G., & Skoog, A. (1995). Dissolved organic matter in Arctic multi-year sea ice during winter: Major components and relationship to ice characteristics. *Polar Biology*, *15*(7), 477–483.
Ushio, S. (2006). Factors affecting fast-ice break-up frequency in Lützow-Holm Bay, Antarctica. *Annals of Glaciology*, *44*, 177–182.
Willmes, S., & Heinemann, G. (2016). Sea-ice wintertime lead frequencies and regional characteristics in the Arctic, 2003–2015. *Remote Sensing*, *8*(1), 4. https://doi.org/10.3390/rs8010004
Zemmelink, H. J., Dacey, J. W. H., Houghton, L., Hintsa, E. J., & Liss, P. S. (2008). Dimethylsulfide emissions over the multi-year ice of the western Weddell Sea. *Geophysical Research Letters*, *35*, L06603. https://doi.org/10.1029/2007GL031847
Zhou, J., Delille, B., Eicken, H., Vancoppenolle, M., Brabant, F., Carnat, G., et al. (2013). Physical and biogeochemical properties in Landfast sea ice (Barrow, Alaska): Insights on brine and gas dynamics across seasons. *Journal of Geophysical Research: Oceans*, *118*(6), 3172–3189. https://doi.org/10.1002/jgrc.20232